Original Research Paper

IJES *Iranian Journal of Earth Sciences*
Vol. 15, No. 3, 2023, 188-194.
DOI: 10.30495/ijes.2023.1973739.1815

Extracting clay minerals with emphasis on Bentonite in Eastern Iran, using Landsat 8 and ASTER images

Saeed Saadat*[1], Maliheh Ghoorchi[1], Rahim Dabiri[1]

1. Department of Petroleum Engineering and Geology, Mashhad Branch, Islamic Azad University, Mashhad, Iran

Received 28 November 2022; accepted 1 February 2023

Abstract

The prospecting area is located in the eastern part of Iran. Aster and Landsat 8 satellite images were processed with different spectral analyses techniques to detect the clay representing the alteration zones, with emphasis on bentonite occurrences in the study area. Band ratio (BR), Spectral Angle Mapper (SAM), Mixture Tuned Matched Filtering (MTMF), Principal Component Analysis (PCA), Spectral Feature Fitting (SFF), and Least Square Fit (LS-Fit) techniques were performed to show the promising areas for clay mineral. Band ratios of 6/7, 6/5, and 4/2 from Landsat 8 OLI imagery and 4/6, 5/6, 5/8, from ASTER were used to enhance clay alterations. The results obtained from the supervised classification using the SAM algorithm for minerals from US Geological Survey spectral library (USGS) have been compared with the results of Jet Propulsion Laboratory (JPL) spectral library. The Sequential Maximum Angle Convex Cone (SMACC) algorithm also performed to detect same minerals. Comparing the different analyzing satellite image based on ASTER data indicate all methods generate relatively similar results for clay mineral. Although all methods generate relatively similar results, the SAM method seems to be the best fit with geological evidences to generate reliable promising areas for clay mineral in this area. Based on this study, around 100 km^2 of the total studied area was selected as suitable for more exploration and ground survey.

Keywords: *Remote sensing, Clay minerals, Bentonite, Iran.*

1. Introduction

Bentonite is a one of the common industrial clays and as known as montmorillonite, which is a sub group of smectite minerals. Bentonite is produced by weathering and erosion of volcanic ash with the major mineral composition of montmorillonite (Sample-Lord et al. 2021). Other assemblage minerals, such as quartz, calcite, feldspar, gypsum, dolomite, and plagioclase may be present.

Bentonite has many uses due to important physical and chemical properties such as crystal structure, chemical composition, small crystal size (large specific surface area), cation exchange, expansibility, colloidal properties, plasticity, dehydration, adsorption, and cohesiveness. The most common applications are in civil engineering, geotechnical engineering, oil drilling, filling, foundry, painting, ceramics, and nanocomposites. Variety of industrial applications are related to concentrations of CaO and Na_2O content in montmorillonite (Saadat and Ghoorchi 2021, and references there in). Remote sensing data have been used in many scientific fields for producing thematic maps especially mineral mapping. ASTER and Landsat data have been used by many researches to display hydrothermal alteration zones, include argillic and advanced argillic mineral mapping. Lamrani et al. (2021) have integrated different remote sensing processing techniques and mineralogical data to map the spatial distribution of clay minerals in the Zeghanghane area, Morocco. Vural et al. (2021) about the mineralogy of clay areas in Gümüşhane (NE Turkey) by remote sensing methods. Aisabokhae and Osazuwa (2021) used Spectral Angle Mapper (SAM), Spectral Feature Fitting (SFF), Constrained Energy Minimization (CEM), and Mixture Tuned Matched Filtering (MTMF) alteration mapping techniques to map the abundance of the identified alteration minerals from ASTER satellite images. Satellite image processing of some bentonite deposits in Sarbisheh area shows argillic alteration with the presence of montmorillonite (Nakhaei et al. 2019). Karimpour and Malek Zadeh (2016) processed ASTER images for recognition of some sodic and calcic type bentonite deposits in Ferdows area (Eastern Iran).

Bentonite deposits in Iran are mainly scattered in 6 regions including: Semnan-Troud, Alborz-Azerbaijan, Eastern Iran, Central Iran, Tafresh-Takab and Zagros (Hejazi and Ghorbani 2013), which most of them are related to Cenozoic volcanic activities, from the beginning of the Eocene to the Pleistocene (Ghorbani 2013).

In this research occurrences of bentonite in East of Iran were determined by using several remote sensing analyses techniques on Landsat and Aster images. Due to the many uses of bentonite, especially in the supply of raw materials for steel industries, which has been greatly expanded in recent years in the east of Iran, the aim of this paper is to find new potential for bentonite deposits in this area. The exploration of undiscovered deposits in other similar regions would be aided by the spatial link between known deposits and the existing alteration zones.

---

*Corresponding author.
E-mail address (es): saeed.saadat@colorado.edu

2. Materials and methods

2.1 Study area

The studied area is located in Eastern Iran and includes parts of South Khorasan provinces (Fig 1). This covers an area of about 3160 square kilometers between longitudes 59°25'49" to 60°1'10" east and latitudes 32°24'14" to 32°55'12" north, in Sarbisheh and Sahl-abad geological maps with a scale of 1:100000 (Navai 1974;Nazari and Salamti 1999).

The Eastern Iran includes a number of structural sub-sets in terms of tectonics and metallogenic zones. Different processes have occurred due to the variety of tectonic and magmatic history from the Precambrian to the present. A very thick row of metamorphic, sedimentary rocks and different intrusive and volcanic igneous rocks has been outcropped (Fig 1). Various tectonic events in eastern Iran, especially the Lut block, have caused a huge volume of magmatic activities (mainly Eocene) with different geochemical characteristics and different mineralization (Karimpour et al. 2011). Bentonite deposits from Eastern Iran were formed through the alteration of intermediate to acidic magmatism with composition from trachy-andesite to rhyolite (Modabberi et al. 2019).

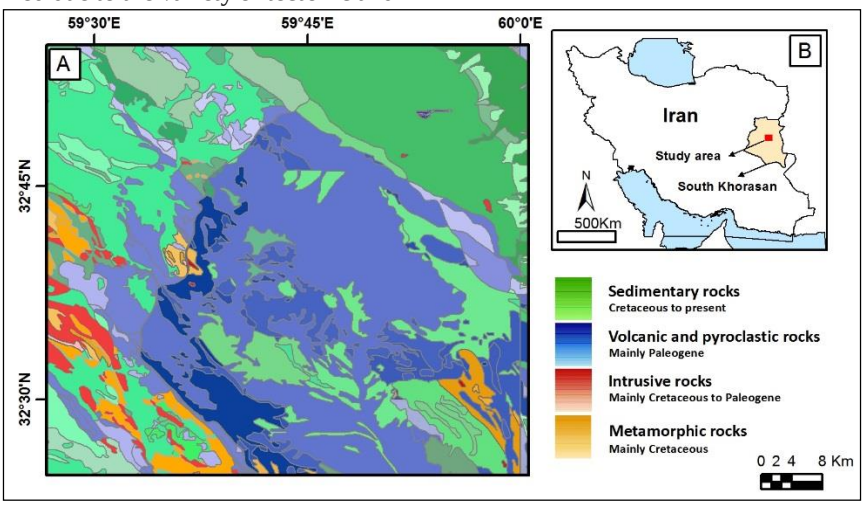

Fig 1. Simplified geological map of study area (based on Birjand 1:250000 geological map)

2.2 Remote Sensing Data

The Landsat 8 and Aster images used to detect occurrences of bentonite. Landsat 8 was launched on 2013, carries the Operational Land Imager (OLI) and the Thermal Infrared Sensor (TIRS) instruments. These satellite images have 30 meters (visible, NIR, SWIR); 100 meters (thermal); and 15 meters (panchromatic) multi-spectral spatial resolutions along a 185 km swath. Landsat 8 was developed as a collaboration between NASA and the U.S. Geological Survey (USGS).

Aster (Advanced Spaceborne Thermal Emission and Reflection Radiometer) was launched on EOS-Terra in 2000. ASTER is a multispectral image and obtains high-resolution images in 14 different wavelengths, ranging from visible (520–860 nm, at a spatial resolution of 15 m), shortwave infrared (1600–2430 nm, at a spatial resolution of 30 m) to thermal infrared bands (8125–11650 nm, at a spatial resolution of 90 m). ASTER images have a higher spectral resolution and provide better detection of alteration zones due to their multiple shortwave infrared bands. The focus on Aster images was on absorption features located in the shortwave infrared (SWIR). The SWIR spectral region are mainly used to detect carbonate, and clay minerals (Rockwell and Hofstra 2008).

2.3 Pre-processing

The Landsat image was acquired by Landsat-8 on 2013 and ASTER image was acquired on 2005 providing L1B-level data. Data processing has been done by ENVI (Environment for Visualizing Images) software. The satellite images were geometrically calibrated. The images were subset spectrally and spatially for processing. The most important steps in preprocessing are the radiometric calibration and atmospheric correction. Satellite images were atmospherically calibrated by Internal Average Relative Reflectance (IARR). The Normalized Difference Vegetation Index (NDVI) has performed to detect the vegetated area, although it may be changed over time. Urban areas were masked for each selected image by using a GIS shape file.

3. Results and discussion

The detection of features in satellite images depends on using the proper spectral bands.

The spectral properties of clay minerals and clay mineral-bearing rocks are important in remote sensing. Reflectance spectra of montmorillonite, hectorite, saponite and nontronite minerals are shown in figure 2. The absorption feature around 2.20 µm is due to the Al–OH component. All smectite spectra exhibit an H_2O stretching, that clearly is identifiable (Fig 2). Montmorillonite with high Al abundance in the

octahedral sites exhibit an OH combination band near 2.20 µm but, with some Fe^{3+} or Mg in the octahedral sites, it can be extended toward 2.21 µm and also longer wavelengths (2.4–2.5 µm) that depends on the octahedral cations (Bishop et al. 2014).

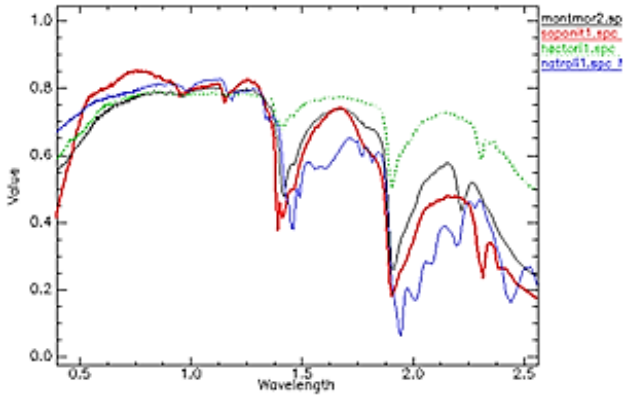

Fig 2. Reflectance spectra of montmorillonite, hectorite, saponite and nantronite minerals (Spectral Library of USGS)

Remote sensing techniques like band ratio, Spectral Angel Mapper, Principal Component Analysis, Mixture Tuned Matched Filtering, Spectral Feature Fitting, and Least Square Fit were employed in this study to discriminate clay minerals with emphasis on bentonite.
Band ratio (BR) is a simple and powerful method that widely used for mineral and lithological mapping (Abrams et al. 1983). It can highlight spectral features between the target and background with respect to the wavelength of absorption and highest reflectance. Band ratios for some clay minerals is shown in Table 1. In this study, band ratios 6/7, 6/5, and 4/2 from Landsat 8 OLI imagery band ratios 4/6, 5/6, 5/8, from ASTER imagery were used to enhance clay alterations (Fig 3).

Table 1. Band ratios for some clay minerals

Mineral	Relative absorption band	Refrence
Muscovite, smectite, illite	(5+7)/6	Mars and Rowan (2006)
Alunite,kaolinite, pyrophylite	(4+6)/5	Rowan and Mars (2003)
Montmorillonite,	(4+6)/7	Fatima et al. (2017)
Illite, muscovite	(4+7)/(6*2)	Mars and Rowan (2011)

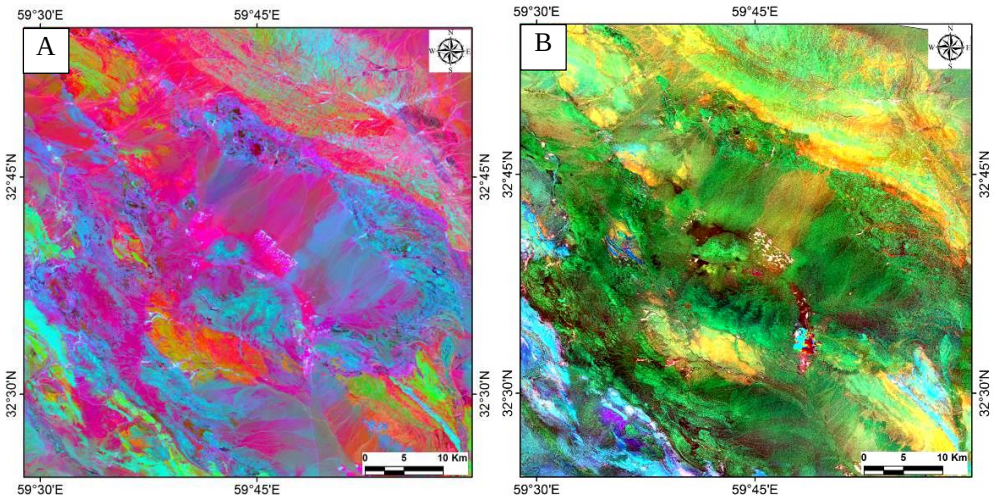

Fig 3. RGB of band ratios: A) 6/7, 6/5, and 4/2 from Landsat 8 OLI imagery, red pixels represent clay minerals. B) 4/6, 5/6, 5/8, from ASTER of study area, yellow pixels represent clay minerals.

Spectral Angel Mapper (SAM) is a rapid mapping classification method that categorizes the images with the "endmembers" to produce mineral maps (Kruse et al. 1993; Dennison et al. 2004). Resampling leads to mixing of spectra and loss of information (Zhou et al. 2003), so detection analysis in this research has done before resampling. SAM is insensitive to scene illumination conditions and therefore can be used on IAR images (Kruse et al. 1993). One of the most important factors, is the appropriate classification thresholds. The SAM classification were performed by different thresholds. The results of detecting montmorillonite using SAM method with Spectral Library of JPL (Jet Propulsion Laboratory) and Spectral Library of USGS (U.S. Geological Survey) is shown in Figure. 4.

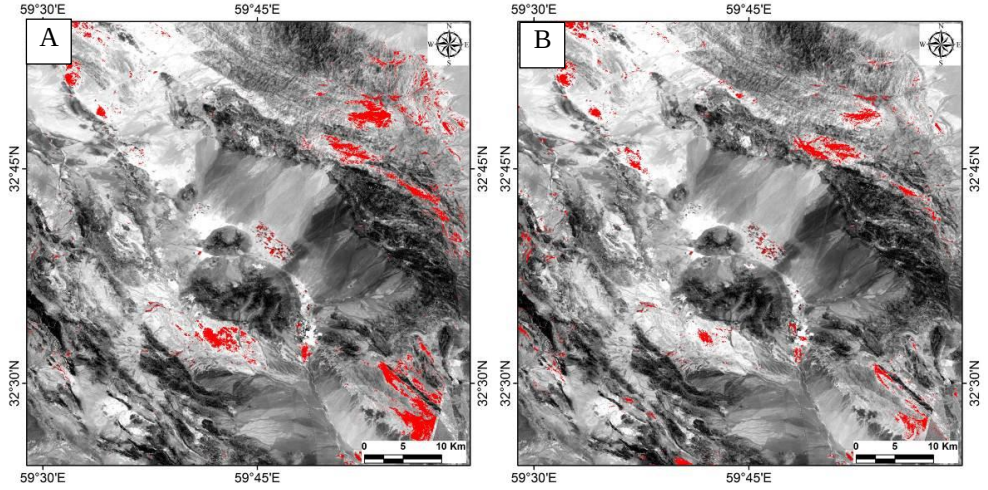

Fig 4. Enhancement of montmorillonite using SAM method with: A) Spectral Library of JPL, and B) Spectral Library of USGS. Red pixel represents the montmorillonite - bearing assemblages.

Red pixel represents the montmorillonite - bearing assemblages resulted from USGS and JPL library.

However, clay minerals are usually mixed with other minerals and they are rarely pure in nature. Ducasse et al. (2020) try to determine the best couple spectral preprocessing/unmixing method, to quantify montmorillonite in mixtures with other minerals, such as kaolinite, illite, calcite and quartz. In this study the Sequential Maximum Angle Convex Cone (SMACC) algorithm used to find abundances of selected endmembers. This algorithm was set for 30 endmembers, building a SMACC spectral library. These endmembers can be extracted from an image or another source. Research has shown that endmembers extracted from an image usually perform best when classifying a single image (Jiang et al. 2020). The results from SMACC for montmorillonite is shown in Figure 5.

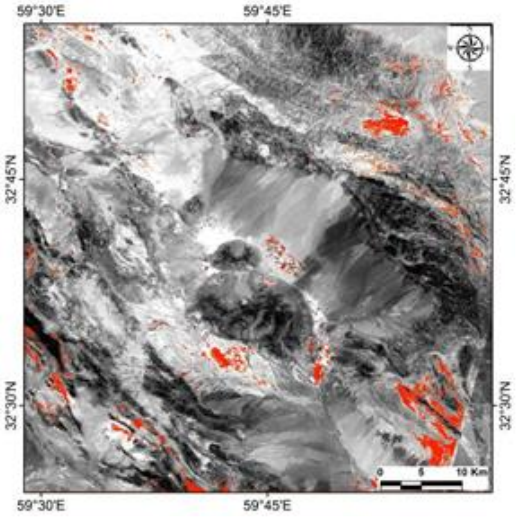

Fig 5. Enhancement of montmorillonite using SMACC algorithm.

The principal component analysis (PCA) can compress highly correlated bands to one band. This method can eliminate the effects of radiation and thus lead to better detection geological phenomena (Crosta et al. 2003). PCA analysis performed on bands number 4, 5, 6 and 7 of Aster images. Combinations of selected PCA band are used for highlighting clay alteration and montmorillonite mineral. PC3 was selected to show montmorillonite based on the value and sign of its eigenvectors (Fig 6A). The respective alterations are shown as brighter white pixels where the darker pixels match other rocks (Fig 6A).

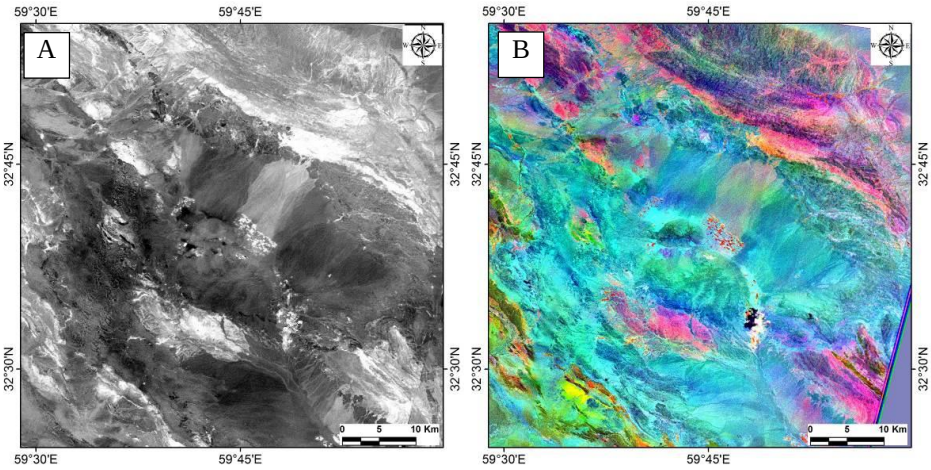

Fig6. A) PC3 image, clay alteration is observable as bright pixels. B) RGB result using all the SWIR bands as the input bands and residual bands b4, b6 and b8 as the modeled band for detecting argillic (pink pixels), propylitic alterations (green pixels).

Least Square Fit (LS-Fit) technique assumes that the bands used as input values are behaving as the variables of a linear expression. The minerals which are sensitive to a specific band are then differentiated from the features which are reflective to the other bands as well; just by taking the difference between the predicted values and the original values (Sarp 2005). This technique was done in the study area by using all the SWIR bands as the input bands and residual bands b4, b6 and b8 as the modeled band for detecting argillic and propylitic alterations (Fig 6B).

Mixture Tuned Matched Filtering (MTMF) is an advanced type of spectral mixture analysis, based on a signal processing procedure that is used for sub-pixel mapping of target alteration minerals (Laeiq et al. 2016). The MTMF algorithm includes three main steps: (1) MNF transformation of apparent reflection data (Green et al. 1988), (2) matched filtering for abundance estimation, and (3) mixture tuning calculation (MT) for the identification infeasible or false-positive pixels. The computation of (MNF) for the input is necessary to reduce the dimension of data. The findings of MTMF technique are accessible as MF and infeasibility that makes it possible to choose the pixels with low infeasibility and high MF (Mundt et al. 2007). The results of detecting montmorillonite with MTMF is shown in Figure 7A.

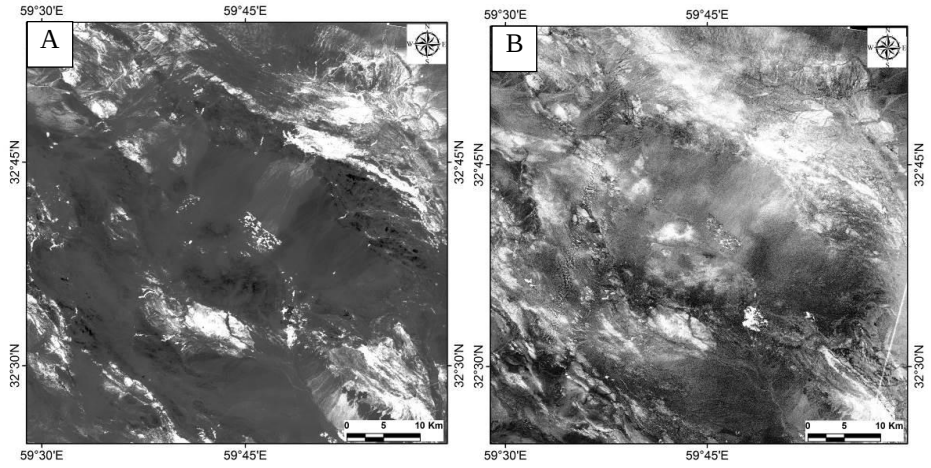

Fig 7. Enhancement of montmorillonite using: A) MTMF method, and B) SFF method for montmorillonite - bearing assemblages.

Spectral feature fitting (SFF) matches the specific absorption features from image spectra to endmembers within a certain wavelength range (Clark 1999). SFF algorithm removes the continuum of absorption feature. The identification of best fitting material depends on spectral features of reference and done by comparing the correlation coefficient of fits (Boardman and Kruse 1994). The results of detecting montmorillonite with SFF method is shown in Figure 7B. The brighter pixels display perfect matching of pixel spectrum with reference spectrum of mineral. The low RMS (Root Mean Square) error are closely matched pixels.

4. Conclusions

Landsat and ASTER data have been used for enhancing areas with clay minerals with emphasis on bentonite in the eastern Iran. Where the ability of Landsat data is limited to identify clay, ASTER data can better distinguish the clay minerals. Comparing the different analyzing satellite image based on ASTER data indicate all methods generate relatively similar reliable promising areas for clay mineral. Target pixels extracted by SAM from USGS library are less than those extracted by other. Based on this study, around 100 km^2 of the total studied area was selected as suitable for more exploration and ground survey.

Acknowledgement

The authors thank the private mining companies for the financial support based on the contract number 1400/195 dated 5/2/2022 with Islamic Azad University, Mashhad branch.

References

Abrams MJ, Brown D, Lepley L, Sadowski R (1983) Remote sensing for porphyry copper deposits in southern Arizona, *Economic Geology* 78:591–604.

Aisabokhae J, Osazuwa I (2021) Radiometric mapping and spectral based classification of rocks using remote sensing data analysis: The Precambrian basement complex, NW Nigeria, Remote Sensing Applications: *Society and Environment* 21, 100447.

Bishop JL, Michalski JR, Carter J (2017) Remote detection of clay minerals. *In Developments in clay science* 8:482-514.

Boardman JW, Kruse FA (1994) Automated spectral analysis: a geological example using AVIRIS data, north Grapevine Mountains, Nevada. Proceedings of the Thematic Conference on Geologic Remote Sensing.

Clark RN (1999) Spectroscopy of rocks and minerals, and principles of spectroscopy. *Man. Remote Sens* 3 (3-58):2-2.

Crosta AP, De Souza Filho CR, Azevedo F, Brodie C (2003) Targeting key alteration minerals in epithermal deposits in Patagonia, Argentina, using ASTER imagery and principal component analysis. *Int J Remote Sens* 24(21):4233–4240.

Dennison PE, Halligan KQ, Roberts DA (2004) A comparison of error metrics and constraints for multiple endmember spectral mixture analysis and spectral angle mapper, *Remote Sens. Environ*. 93:359–367.

Ducasse E, Adeline K, Briottet X, Hohmann A, Bourguignon A, Grandjean G (2020) Montmorillonite estimation in clay–quartz–calcite samples from laboratory SWIR imaging spectroscopy: A comparative study of spectral pre-processing and unmixing methods, *Remote Sensing* 12(11):1723.

Fatima K, Khattak MUK, Kausar AB, Toqeer M, Haider N, Rehman AU (2017) Minerals identification and mapping using ASTER satellite image, Journal of Applied *Remote Sensing* 11:46006.

Green AA, Berman M, Switzer P, Craig MD (1988) A Transformation for Ordering Multispectral Data in Terms of Image Quality with Implications for Noise Removal, IEEE *Transactions on Geoscience and Remote Sensing* 26: 65–74.

Hejazi M, Ghorbani M (2013) Geology of Iran (bentonite and zeolite deposits), Geological Survey and Mineral Exploration of Iran 108 p.

Jiang T, Werff H, Meer F (2020) Classification Endmember Selection with Multi-Temporal Hyperspectral Datam *Remote Sens* 15;12(10):1575.

Karimpour M, Malek Zadeh Shafaroodi A (2016) Satellite Mineral Mapping for Recognition of Sodic and Calcic Type Bentonite Deposits in Eastern Iran, *Advanced Applied Geology* 6(3):84-96.

Karimpour MH, Stern CR, Farmer L, Saadat S, Malekezadeh A (2011) Review of age, Rb-Srgeochemistry and petrogenesis of Jurassic to Quaternary igneous rocks in Lut Block, Eastern Iran, *Geopersia* 1(1):19-36.

Kruse FA, Lefkoff AB, Boardman JW, Heidebrecht KB, Shapiro AT, Barloon PJ, Goetz AFH (1993) The spectral image processing system (SIPS)-interactive visualization and analysis of imaging spectrometer data, Remote Sens. *Environ* 44:145-163.

Laeiq A, Tahir S, Khan SD (2016) Reflectance spectroscopy and remote sensing data for finding sulfidebearing alteration zones and mapping geology in GilgitBaltistan, Pakistan, Earth Sci. *Inform* 9(1): 113-121.

Lamrani O, Aabi A, Boushaba A, Seghir MT, Adiri Z, Samaoui S (2021) Bentonite clay minerals mapping using ASTER and field mineralogical data: A case study from the eastern Rif belt, Morocco, Remote Sensing Applications: *Society and Environment* 24:100640.

Mars JC, Rowan LC (2006) Regional mapping of phyllic- and argillic-altered rocks in the zagros magmatic arc, Iran, using advanced spaceborne thermal emission and reflection radiometer (ASTER) data and logical operator algorithms, *Geosphere* 2:161–186.

Mars JC, Rowan LC (2011) ASTER spectral analysis and lithologic mapping of the Khanneshin carbonatite volcano, Afghanistan, *Geosphere* 7(1): 276–289.

Modabberi S, Namayandeh A, Setti M, López-Galindo A (2019) Genesis of the Eastern Iranian bentonite deposits, *Applied Clay Science* 168:56-67.

Mundt JT, Streutker DR, Glenn NF (2007) Partial Unmixing of Hyperspectral Imagery: Theory and methods, ASPRS Annual Conference Tampa, Florida 1-12.

Nakhaei M, Mohammadi SS, Rasa I, Samiee S (2019) Study of mineralogy, geochemistry and elemental behavior in the process of bentonites formation in Sarbisheh area (South Khorasan, east of Iran), *Iranian Journal of Crystallography and Mineralogy* 27(1):207-220.

Navai I (1974) Geological map of Sahl-abad, sheet 7954, scale 1:100,000, Geological Survey of Iran, Tehran.

Nazari H, Salamti R (1999) Geological map of Sarbisheh, sheet 7955, scale 1:100,000, Geological Survey of Iran, Tehran.

Rockwell BW, Hofstra AH (2008) Identification of quartz and carbonate minerals across northern Nevada using ASTER thermal infrared emissivity data—Implications for geologic mapping and mineral resource investigations in well-studied and frontier areas, *Geosphere* 4(1):218-246.

Rowan LC, Mars JC (2003) Lithologic mapping in the Mountain Pass, California area using advanced spaceborne thermal emission and reflection radiometer (ASTER) data, *Remote sensing of Environment* 84(3):350-366.

Sample-Lord KM, Ahmed M, Malusis MA (2021) Diffusion through soil-bentonite backfill from a constructed vertical cutoff wall, *Soils Found* 61:429–443.

Saadat S, Ghoorchi M (2021) Exploration of industrial minerals (remote sensing, geochemistry, geophysics, geology and environment), Islamic Azad University Publications, Mashhad branch, 536 pp.

Sarp G (2005) Lineament analysis from satellite images, north-west of Ankara, Master's thesis, Middle East Technical University.

Vural A, Akpinar İ, Sipahi F (2021) Mineralogical and Chemical Characteristics of Clay Areas, Gümüşhane Region (NE Turkey), and Their Detection Using the Crósta Technique with Landsat 7 and 8 Images, *Nat Resour Res* 30:3955–3985.

Zhou Q, Jing Z, Jiang S (2003) Remote Sensing Image Fusion for Different Spectral and Spatial Resolutions with Bilinear Resampling Wavelet Transform, In Proceedings of the IEEE Conference on Intelligent Transportation Systems (ITSC) Shanghai, *China* 2:1206–1213.